Supporting Information

Role of Supramolecular Polymers in Photo-actuation of Spiropyran Hydrogels

Chuang Li[1,2†], Qinsi Xiong[4†], Tristan D. Clemons[2,4], Hiroaki Sai[2,5], Yang Yang[2], M. Hussain Sangji[2,6], Aysenur Iscen[2,3,§], Liam C. Palmer[2,4,8], George C. Schatz[3,4*], Samuel I. Stupp[2,4,5,6,7,8*]

Author Address

[1] Department of Polymer Science and Engineering, University of Science and Technology of China, Hefei, Anhui, 230026 P. R. China.

[2] Center for Bio-inspired Energy Science, Northwestern University, 2145 Sheridan Road, Evanston, IL 60208, USA.

[3] Department of Chemical and Biological Engineering, Northwestern University, 2145 Sheridan Road, Evanston, IL 60208, USA.

[4] Department of Chemistry, Northwestern University, 2145 Sheridan Road, Evanston, IL 60208, USA.

[5] Department of Materials Science and Engineering, Northwestern University, 2220 Campus Drive, Evanston, IL 60208, USA.

[6] Department of Biomedical Engineering, Northwestern University, 2145 Sheridan Road, Evanston, IL 60208, USA.

[7] Department of Medicine, Northwestern University, 676 N St. Clair, Chicago, IL 60611, USA.

[8] Simpson Querrey Institute, Northwestern University, Chicago, 303 E. Superior Street, IL 60611, USA.

[§] Present address: Max Planck Institute for Polymer Research, Ackermannweg 10, Mainz 55128, Germany.

[†] These authors contributed equally to this work.

[*] Correspondence to: g-schatz@northwestern.edu; s-stupp@northwestern.edu.

Outline

Section 1. Synthesis of peptide amphiphile (PA)

Solid-phase peptide synthesis was conducted using Rink Amide MBHA resin (100-200 mesh, 0.50 mmol/g). Fmoc deprotections were performed with 30% 4-methylpiperidine in DMF solution for 10 min and Mtt deprotections were performed with trifluoroacetic acid (TFA)/triisopropylsilane (TIS)/dichloromethane in a volumetric ratio of 5:1:94 for 5 min. Amino acid coupling reactions were carried out using a coupling mixture of amino acid/HBTU/DIEA (4 : 3.95 : 6 relative to the resin) in DMF. Cleavage of the peptides from the resin was carried out with a mixture of TFA/TIS/H_2O in a volumetric ratio of 95:2.5:2.5 for 3 hours. After removal of excess TFA by rotary evaporation, the remaining peptide solution was triturated with cold diethyl ether to obtain a slightly yellow precipitate solid, followed drying under vacuum overnight. The peptides were purified by preparative reverse phase HPLC using a Phenomenex Gemini column (C_{18}, 10 µm, 100 Å, 30×150 mm) at 25 ºC on a Varian Prostar Model 210 preparative HPLC system. Water/acetonitrile gradient containing 0.1 vol % NH_4OH was used as an eluent at a flow rate of 25 mL/min. The purified fractions were collected and concentrated by rotary evaporation to remove acetonitrile, then lyophilized and stored at -20 ºC. Products were characterized by electrospray ionization mass spectrometry (ESI-MS) using an Agilent 6510 quadrupole time-of-flight (Q-TOF) instrument, with 0.1% NH_4OH in a water/acetonitrile mix (70:30) as eluent.

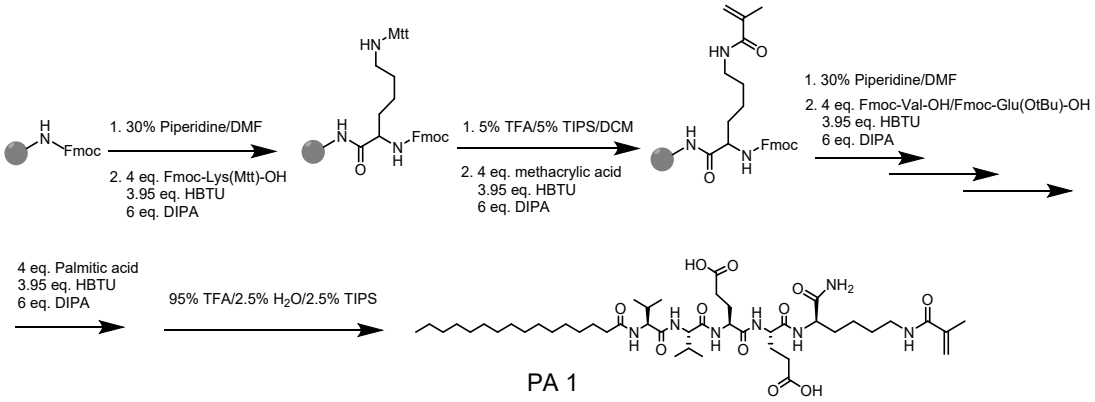

Scheme S1. Solid-phase synthesis of peptide amphiphiles.

In total, six peptide sequences were synthesized and characterized:

PA 1: C_{16}VVEEK-Methacrylamide, Calc. 908.19, found $[M+H]^+$ 909.67.

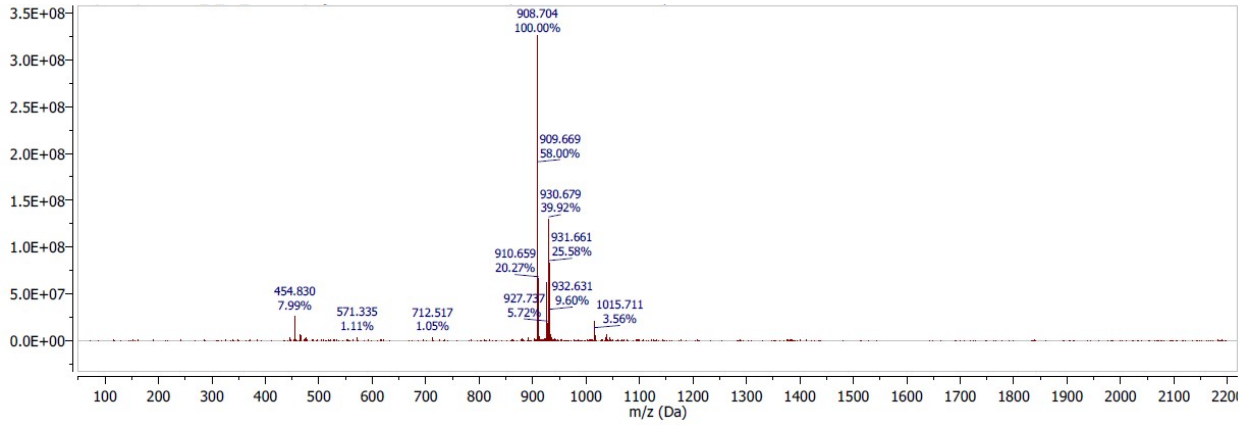

PA 2: C_{16}VVEE-NH_2, Calc. 711.94, found $[M-H]^-$ 710.64.

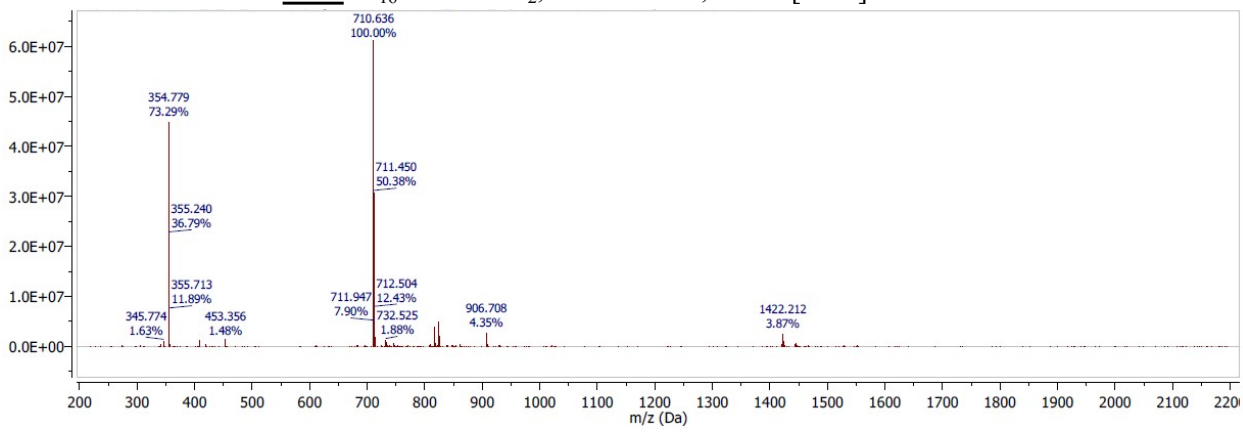

PA 3: C_{16}VEVEK-Methacrylamide, Calc. 908.19, found $[M+Na]^+$ 930.70.

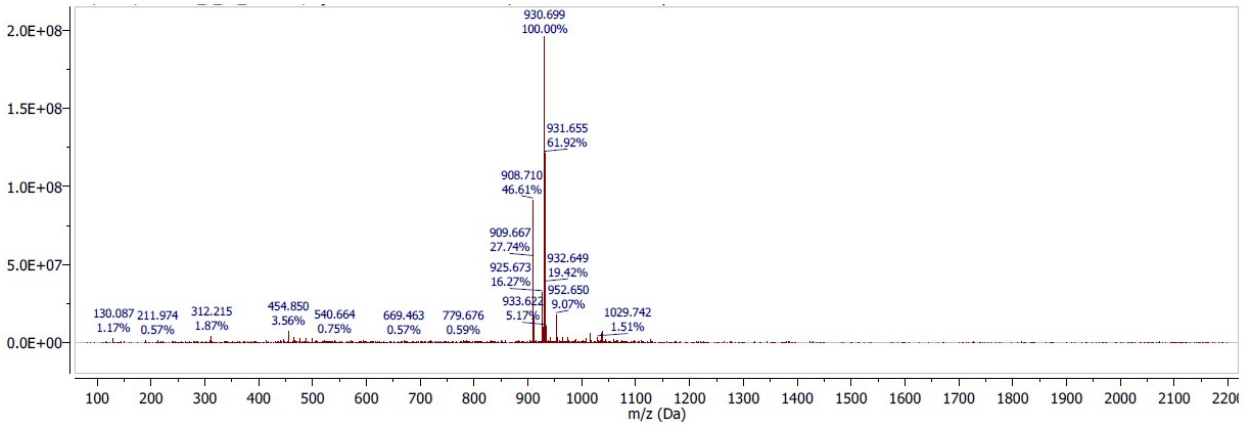

PA 4: C_{16}VEVE-NH_2, Calc. 711.94, found $[M-H]^-$ 710.60.

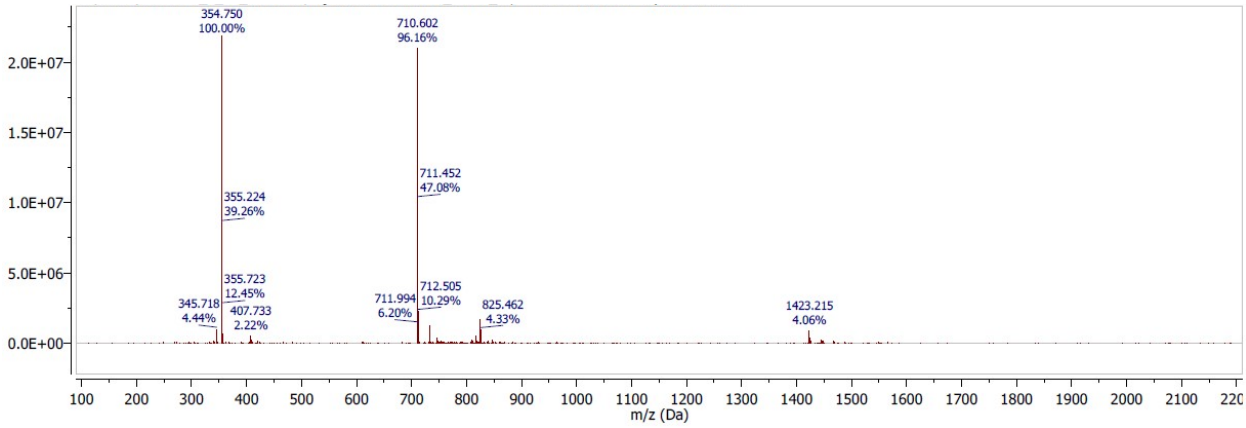

PA 5: C_{16}EEEEK-Methacrylamide, Calc. 968.16, found $[M-H]^-$ 966.82.

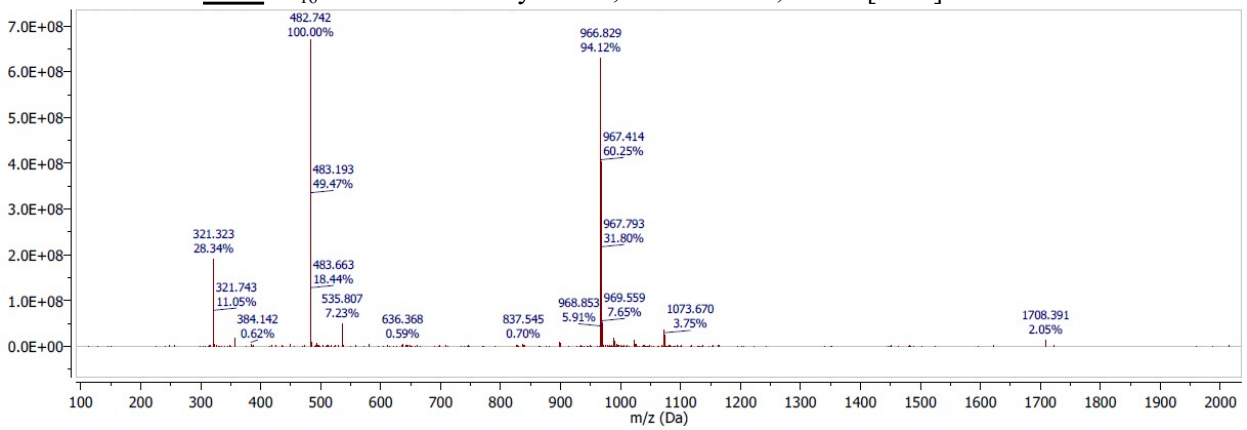

PA 6: C_{16}EEEE-NH_2, Calc. 771.91, found $[M+H]^+$ 772.66.

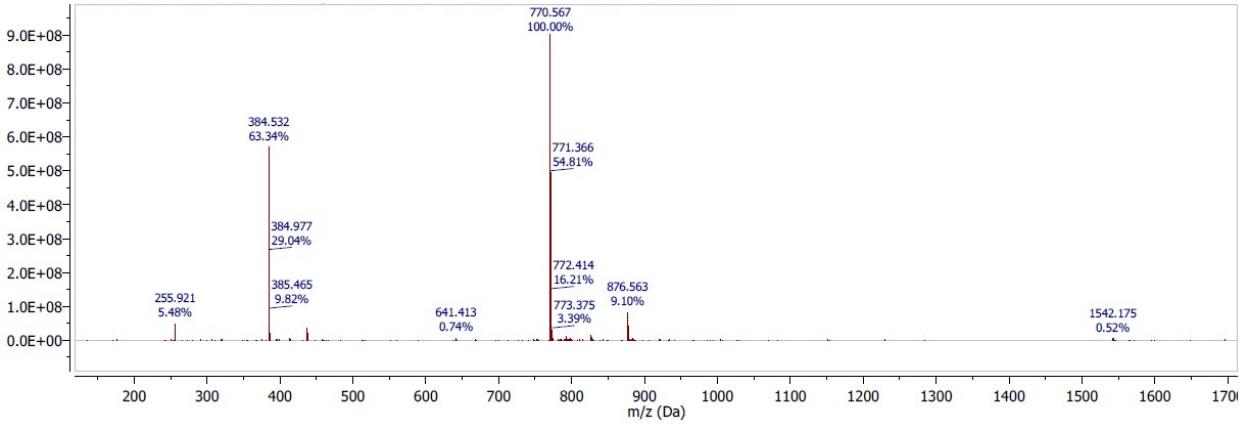

Section 2. Self- and co-assembly of PAs

For self-assembly, peptide amphiphiles were added to water to give a final concentration of 10 mM and 1 equiv. NaOH was added to help dissolve the PAs. The solutions were annealed by heating in a water bath at 80 °C for 30 min, followed by cooling to room temperature overnight. For co-assembly, methacrylate PA (PA 1, or 3, or 5) and filler PA (PA 2, or 4, or 6) were dissolved in water with a molar ratio of 1:1 to give a total PA concentration of 10 mM and 1 equiv. NaOH was added to help dissolve the PAs. The solution was annealed following the same procedure described above.

Cryogenic Transmission Electron Microscopy (Cryo-TEM)

300-mesh copper grids with lacey carbon film (Electron Microscopy Sciences, Hatfield, PA, USA) were glow discharged for 30 seconds in a PELCO easiGlow system (Ted Pella, Inc., Redding, CA, USA) prior to use. 7 μL of sample solutions at a PA concentration of 1mM were transferred to the plasma-cleaned 300-mesh copper grids with lacey carbon support and plunge-frozen using a Vitrobot Mark IV (FEI) vitrification robot. Samples were blotted at room temperature with 95-100% humidity and plunged frozen into liquid ethane. Samples were transferred into a liquid nitrogen bath and placed into a Gatan 626 cryo-holder through a cryo-transfer stage. Cryo-TEM was performed using a liquid nitrogen cooled JEOL 1230 TEM working at 100 kV accelerating voltage. Images were acquired using a Gatan 831 CCD camera.

Atomic force microscopy

The annealed samples were diluted to 1 mM in water and cast to mica substrate followed by fixing with a $CaCl_2$ solution (400 mM) and washing with DI water for three times. The samples were measured using a Dimension Icon Atomic force microscopy (Bruker).

X-ray scattering measurements

Two-dimensional small-angle X-ray scatting (SAXS) measurements were performed at the 5-ID-D beamline of the DuPont-Northwestern-Dow Collaborative Access Team (DND-CAT) Synchrotron Research Center at the Advanced Photon Source, Argonne National Laboratory. Samples were sealed in a glass capillary with 1 mm diameter before measurement. Air background and water background scattering patterns were obtained and used for background subtraction. Data was collected using an energy of 17 keV and a CCD detector positioned 245 cm behind the sample. Data reduction from the 2D scattering patterns to 1D scattering profiles were conducted with GSAS-II, and the data analysis was performed with the Irena software package running on Igor Pro software.

Dynamic Light Scattering (DLS) measurements

The annealed samples were diluted to 0.1 mM in water and transferred into a Malvern capillary cuvette, followed by measurements using the Zetasizer Nano (Malvern Panalytical) with a light source of He-Ne laser 633nm.

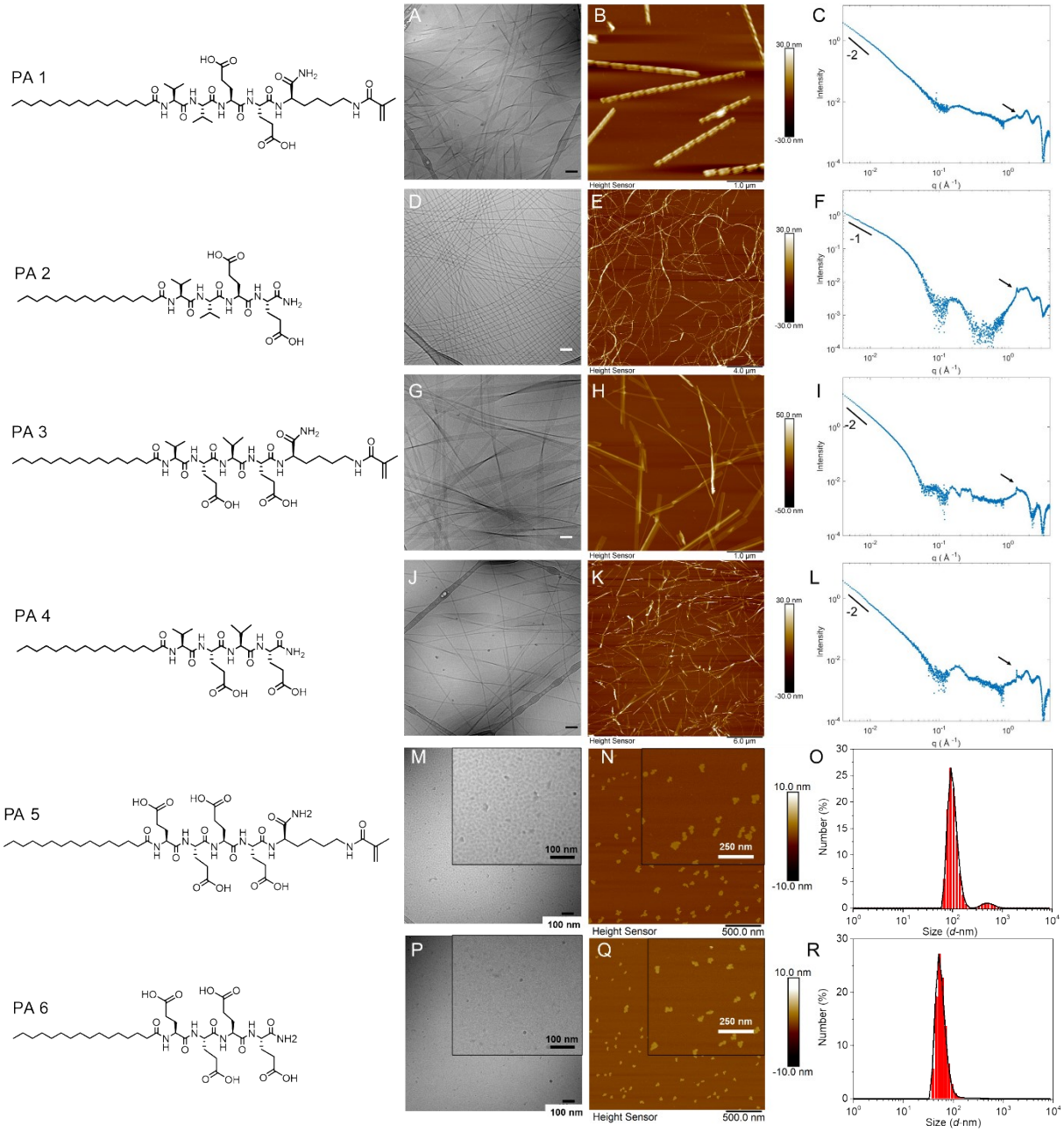

Figure S1. Characterization of self-assembled structures formed by PA**1**-PA**6**. Representative Cryo-TEM images of self-assembly morphology of PA **1** (**A**), PA **2** (**D**), PA **3** (**G**), PA **4** (**J**), PA **5** (**M**) and PA **6** (**P**). Representative AFM images of self-assembly morphology of PA **1** (**B**), PA **2** (**E**), PA **3** (**H**), PA **4** (**K**), PA **5** (**N**) and PA **6** (**Q**). SAXS profiles of self-assembly of PA **1** (**C**), PA **2** (**F**), PA **3** (**I**) and PA **4** (**L**) showing the background-subtracted scattered intensity versus the scattering vector *q* (log–log plot). The black arrow indicates the characteristic β-sheet peak of PA. Dynamic light scattering plots of self-assembly of PA **5** (**O**) and PA **6** (**R**).

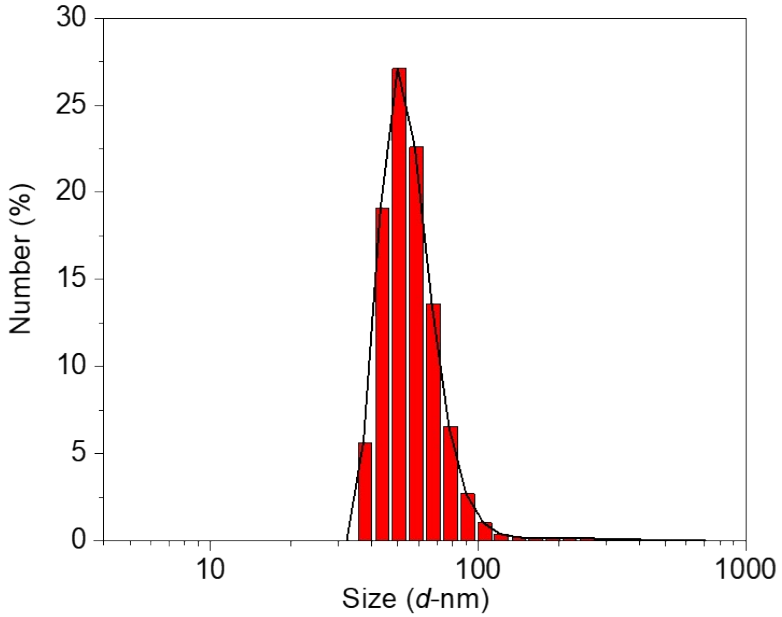

Figure S2. Dynamic light scattering plots of co-assembly of PA **5** and PA **6** mixed in a 1:1 molar ratio of in aqueous solution (0.1 mM in total).

Section 3. Preparation and characterization of PA hybrid hydrogels

3.1 Synthesis of spiropyran molecules

Spiropyrans C1 and C2 were synthesized following our previously reported procedures[1] (summarized in Scheme S2) and purified using an automatic column chromatography instrument (CombiFlash® EZ Prep). ^{1}H and ^{13}C nuclear magnetic resonance (NMR) spectra were acquired on an Agilent DD 600 MHz with an HCN cryoprobe. Electrospray ionization mass spectrometry (ESI-MS) studies were carried out using an Agilent 6510 quadrupole time-of-flight (Q-TOF) instrument. The ^{1}H-NMR, ^{13}C-NMR and ESI-MS spectra data below match those reported previously[1].

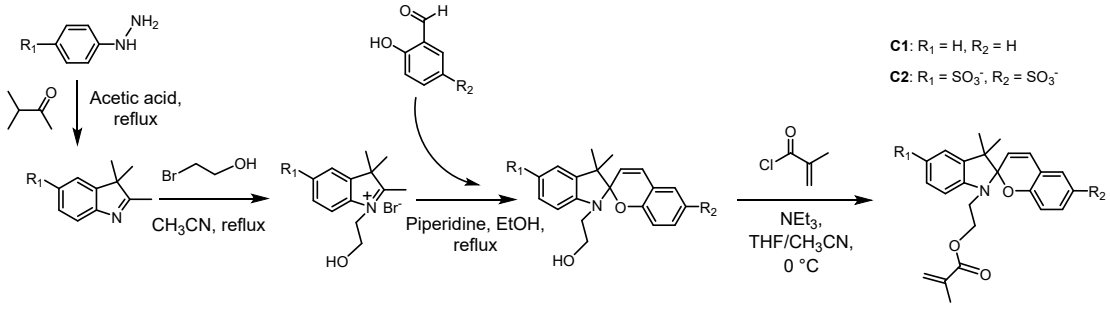

Scheme S2. Synthesis of spiropyran molecule C1 and C2.

2-(3', 3'-dimethylspiro[chromene-2, 2'-indolin]-1'-yl) ethyl methacrylate (C1, 52%)

^{1}H-NMR (500 MHz, $CDCl_3$) δ (ppm): 7.18 (t, 1H), 7.02-7.11 (m, 3H), 6.80-6.88 (m, 3H), 6.66-6.70 (m, 2H), 6.09 (s, 1H), 5.67-5.71 (d, 1H), 5.55 (s, 1H), 5.98 (s, 1H), 4.27-4.33 (m, 2H), 3.37-3.64 (m, 2H), 1.93 (s, 3H), 1.30 (s, 3H), 1.15 (s, 3H).

^{13}C-NMR (500 MHz, $CDCl_3$) δ (ppm): 167.31, 154.11, 147.23, 136.38, 136.20, 129.82, 129.48, 127.57, 126.79, 125.73, 121.74, 120.21, 119.54, 119.25, 118.49, 115.09, 106.47, 104.47, 63.02, 52.23, 42.43, 25.86, 20.09, 18.40.

MS-ESI (m/z): [M] calc. for $C_{24}H_{25}NO_3$ 375.47; $[M+H]^+$ found 376.20.

1'-(2-(methacryloyloxy) ethyl)-3', 3'-dimethylspiro[chromene-2, 2'-indoline]-5', 6-disulfonate (C2, 49%)

^{1}H-NMR (500 MHz, DMSO-d_6) δ (ppm): 7.40 (d, 1H), 7.35-7.38 (m, 1H), 7.26-7.30 (m, 2H), 7.01-7.04 (d, 1H), 6.56-6.60 (m, 2H), 5.99 (s, 1H), 5.73-5.76 (d, 1H), 5.65 (t, 1H), 4.12-4.30 (m, 2H), 3.34-3.48 (m, 2H), 1.84 (s, 3H), 1.15 (s, 3H), 1.04 (s, 3H).

^{13}C-NMR (500 MHz, DMSO-d_6) δ (ppm): 174.72, 167.32, 154.43, 147.95, 141.69, 140.42, 136.57, 135.92, 130.27, 128.17, 126.92, 126.12, 125.41, 120.35, 120.14, 118.12, 114.42, 105.55, 63.43, 52.54, 42.88, 26.32, 20.38, 18.93.

MS-ESI (m/z): [M] calc. for $C_{24}H_{23}NO_9S_2^{2-}$ 535.58; $[M-2H]^{2-}$ found 266.41.

The UV-Vis absorbance spectra of **C1** and **C2** (0.05 mM in methanol/water (4:1, v/v) containing 5 mM of HCl) were collected both in the dark and after light irradiation (450 nm, 0.35 mW/cm^2, 10 min) using a Shimadzu UV-1800 UV spectrophotometer.

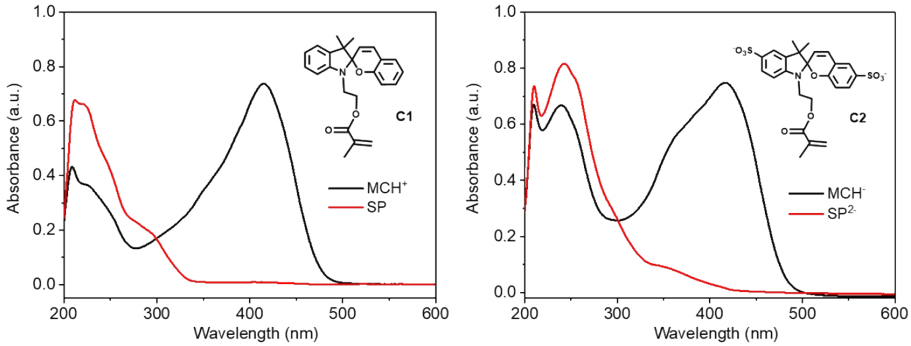

Figure S3. UV-Vis spectra of spiropyran (C1, C2, 0.05 mM) before and after irradiation with 450 nm light.

3.2 Hydrogel preparation

As a representative example of the sample preparation, the VVEE (0.5 wt%) hybrid hydrogel containing C1, *N*-isopropylacrylamide (NIPAAm, 100 mg, 885.0 μmol), *N*,*N*-methylenebisacrylamide (MBAAm, 3.8 mg, 24.7 μmol), C1 (6.64 mg, 17.7 μmol), PA 1 (2.8 mg, 3.1 μmol) and PA 2 (2.2 mg, 3.1 μmol) were dissolved in 1 ml of dioxane/water solvent (4/1, v/v). After heating in a water bath at 80 ºC for 30 min followed by slow cooling to room temperature overnight, a physical gel was obtained. This gel was agitated with a Vortex mixer to break the physical gel. 10 wt% ammonium persulfate initiators (APS, 50 μL) and tetramethylethylenediamine (TEMED, 3.7 μL) were added into the solution to initiate the polymerization at room temperature. After 2 hours, the resulting gel was soaked in a large volume of methanol for 24 h with exchange of fresh solvent every 4 hours to remove residual organic solvent and any unreacted starting materials. The gel was then soaked in water for another 24 h to obtain the final hydrogel. Specific hydrogel samples were prepared following the same procedure by varying hydrogel shapes, PA compositions or PA contents. Blank hydrogels without PA components were prepared following the same procedure.

i. Hydrogel thin films with different PA total contents (0 wt%, 0.5 wt%, 1.0 wt%, 1.5 wt%, 2.0 wt%), or different spiropyran molecules (C1, C2), or different PA compositions (VVEE, VEVE, EEEE), were prepared following the protocol above using a glass mold with a 0.5 mm thick spacer.

ii. Cross-shaped hydrogel films were punched to the desired shape in the swollen state using a high-strength acrylonitrile-butadiene-styrene punch that was 3D-printed using a Stratasys Connex 350 printer.

iii. Rod-shaped hydrogels with a length of approximately 50 mm were prepared by polymerization in a glass capillary with a diameter of 1 mm and removed from the capillary by air pressure.

Table S1 Formulations for preparation of hybrid and covalent hydrogels containing C1 or C2.

Monomers	VVEE hybrid	VEVE hybrid	EEEE hybrid	Covalent soft	Covalent stiff
NIPAAm	100 mg	100 mg	100 mg	100 mg	100 mg
MBAAm	3.8 mg	3.8 mg	3.8 mg	3.8 mg	13.6 mg
C1 (or C2)	6.64 mg (or 9.47 mg)	6.64 mg (or 9.47 mg)	6.64 mg (or 9.47 mg)	6.64 mg (or 9.47 mg)	6.64 mg (or 9.47 mg)
PA 1	2.8 mg	×	×	×	×
PA 2	2.2 mg	×	×	×	×
PA 3	×	2.8 mg	×	×	×
PA 4	×	2.2 mg	×	×	×
PA 5	×	×	2.8 mg	×	×
PA 6	×	×	2.2 mg	×	×
Solvent (dioxane/water, 4/1, v/v)	1 ml	1 ml	1 ml	1 ml	1 ml
APS	100 µl	100 µl	100 µl	100 µl	100 µl
TEMED	3.7 µl	3.7 µl	3.7 µl	3.7 µl	3.7 µl

3.3 Rheology

Mechanical properties of hydrogels were measured using an Anton Paar Modular Compact Rheometer (MCR 302). The hydrogel films (0.5 mm thick) were punched into a dish shape with a diameter of 8 mm and the rheological experiments were performed in 8 mm parallel-plate geometry with a gap size of 0.4 mm at a fixed frequency of 1 Hz and strain of 1% at 25 ºC.

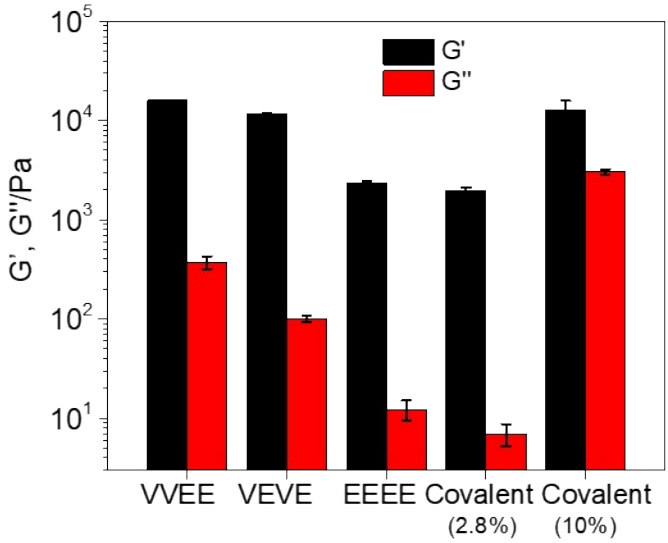

Figure S4. Storage and loss moduli of hybrid hydrogels with 0.5 wt% of the supramolecular components as well as covalent hydrogels with different crosslinker densities (soft, 2.8% crosslinker; stiff, 10% crosslinker).

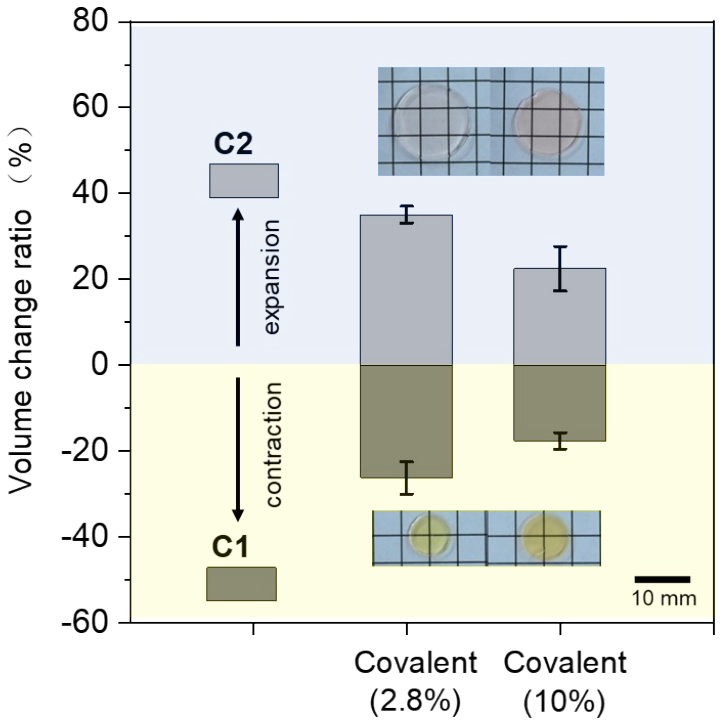

Figure S5. Plot of the net volume change of pure covalent hydrogels with different crosslinking density upon irradiation. Insets show photographs of C2 expanding (top) and C1 contracting (bottom) hydrogels after irradiation.

Section 4. Computational methods

4.1. All-atom simulations

To build the PA nanostructures of our system, we first simulated PA assembly using an all-atom model. Two amphiphilic tetrapeptides with different morphologies were constructed, namely Val-Val-Glu-Glu(VVEE) and Glu-Glu-Glu-Glu(EEEE). In each PA chain, the N terminus was capped with a 16-carbon palmitoyl tail while the C termini was amidated. By following the self-assembly of peptide amphiphiles under neutral pH in experiments, each VVEE PA chain has a net charge of -2 while the EEEE PA chain has a net charge of -4. A VVEE PA with a cylindrical nanofiber morphology was constructed by following the method in Lee *et al*[1]. Nine PA molecules were placed radially in each layer and 12 layers were stacked with a distance of 5 Å and rotated angle of 20°, to create a cylindrical nanostructure composed of 108 PA chains. The Packmol package[2] was used to build the micelle morphology of EEEE PAs, which also included 108 PA chains. Visual Molecular Dynamics[3] (VMD) was used to solvate the structure with a TIP3P water model[4] in a box with dimensions of 120 Å × 120 Å × 60 Å with 0.15 M NaCl. The CHARMM36 force field[5] was applied to simulate the self-assembly of PAs and the NAMD 2.13 software[6] was used to perform the AAMD simulations. All the systems were subject to a 5000 step energy minimization followed by a 10 ns heating and 40 ns cooling with a NPT ensemble at 353–310 K and 1 atm using the Langevin piston[7] Nose-Hoover method[8] implemented in NAMD. The temperature was kept with a damping coefficient of 5 ps^{-1} by using Langevin dynamics while the pressure was kept at 1 atm with a Langevin piston period of 100 fs and a damping time constant of 50 fs. The particle mesh Ewald method[9] was employed to calculate electrostatic interactions with a short-range cutoff of 1.2 nm. Periodic boundary conditions were employed, and with a simulation time step of 2 fs using the SHAKE algorithm. In the production run, a 100 ns simulation was operated using the same settings. The equilibrated PA structures (Figure S6) were subsequently used as the starting structures of supramolecular-covalent hybrid structures in the subsequent coarse-grained model.

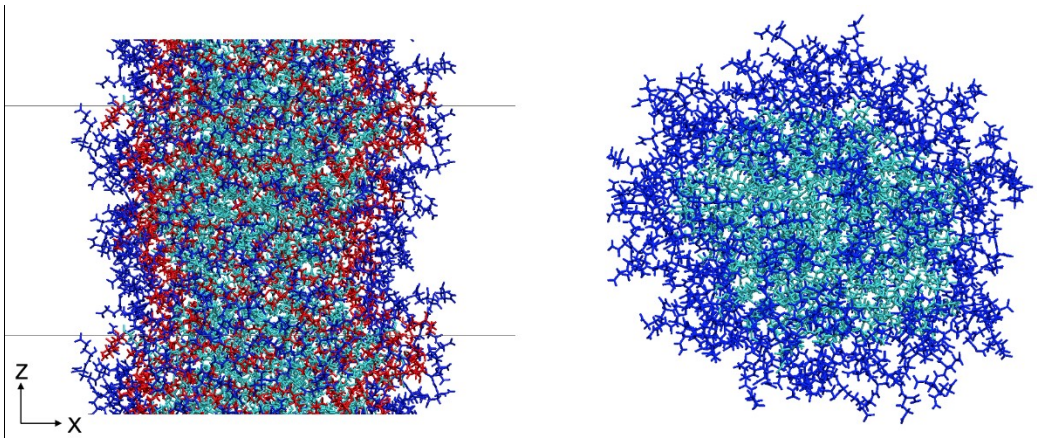

Figure S6. Equilibrated all-atom PA nanofiber (left) and micelle (right) assembled from VVEE and EEEE PAs. The hydrophobic core of PA is shown in cyan, while the VAL amino acid is shown in red and the GLU amino acid is shown in blue. The gray horizontal lines show the periodic boundaries along Z.

4.2. Coarse-grained model and simulations

Parameters used in our CG model were based on our previous work[10–12] and Martini[13] bead types were used to model the PA(VVEE and EEEE), spiropyran (SP and MCH) and NIPAM monomers (see **Figure S7** for bead types). In order to study the behavior of a supramolecular-covalent hybrid network under different supramolecular morphologies and covalent networks with different functional groups (R_1, R_2), we performed a series of molecular dynamics (MD) simulations. The simulation setup for each system modeled with Martini is summarized in **Table S2**.

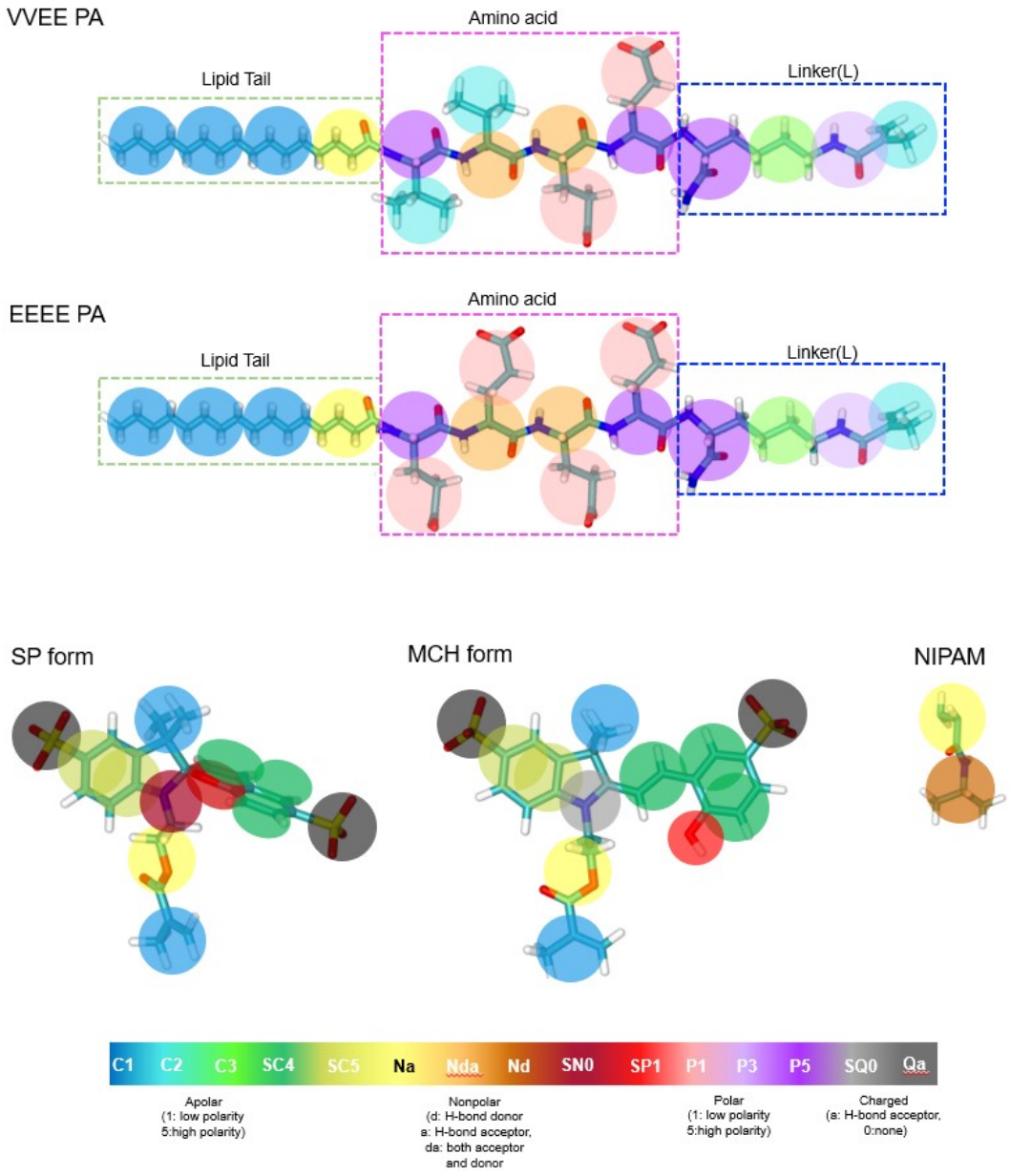

Figure S7. The chemical structures and Martini bead types for PA1 and PA5, spiropyran in light (SP form) and dark (MCH form) conditions and NIPAM monomers. MCH^- and SP^{2-} molecules containing two sulfonate groups are shown here. Here we use the Qa bead type to represent sulfonate group.

Table S2. Summary of simulations using coarse-grained model developed in this study.

System		Number of PA/polymer/CR	Box Size (nm^3)	Number of particles	Simulation time (μs)[a]
VVEE hybrid PNIPAM polymers	MCH^+	108 VVEE + 54 polymer chains + 2.8 CR%	50*50*5.7	367648	RUN1: 1.79; RUN2: 2.40; RUN3: 1.78
	SP			367864	RUN1: 1.75; RUN2: 1.86; RUN3: 1.58
	MCH^-			367468	RUN1: 1.77; RUN2: 2.52; RUN3: 1.94
	SP^{2-}			367252	RUN1: 1.91; RUN2: 1.88; RUN3: 1.76
EEEE hybrid PNIPAM polymers	MCH^+	108 EEEE + 54 polymer chains + 2.8 CR%	38*38*38	1426264	RUN1: 1.66; RUN2: 1.51; RUN3: 1.40
	SP			1426480	RUN1: 1.61; RUN2: 1.52; RUN3: 1.41
	MCH^-			1426126	RUN1: 1.66; RUN2: 1.54; RUN3: 1.40
	SP^{2-}			1425910	RUN1: 1.62; RUN2: 1.52; RUN3: 1.40
Soft control	MCH^+	54 polymer chains + 2.8% CR	30*30*30	698278	RUN1: 1.93; RUN2:2.10
	SP			698494	RUN1: 1.87; RUN2:2.04
	MCH^-			698797	RUN1: 2.19; RUN2:1.97
	SP^{2-}			698581	RUN1: 2.08; RUN2:1.69
Stiff control	MCH^+	54 polymer chains + 10 %CR	30*30*30	698436	RUN1:1.98; RUN2:1.62
	SP			698652	RUN1: 2.67; RUN2:2.05
	MCH^-			1697992	RUN1:2.60; RUN2:1.60
	SP^{2-}			696987	RUN1:1.93; RUN2:1.97

(a) Due to the stochastic nature of the self-assembly processes, the time needed for observing the assembled structures varied significantly in different simulations. To save computation resource, we stopped the simulations if the assembled structures and related morphology properties (SASA, volume, etc.) were maintained for a period of ~300 ns. Therefore, there is a variation of simulation time for different runs of the same type of simulation.

In the supramolecular-covalent hybrid systems, PA nanostructures were obtained based on an AA-to-CG mapping method, as shown in **Figure S7**. Due to the acid pH environment conditions in the PA-covalent hybrid systems (see section 5 Characterization of photoactuation behaviors for more details), Glu residues in PA were protonated. One thing we need to mention is that the pH was different when we made the peptide amphiphile assembly and the PA-covalent hybrid system in our experiment, and our simulation also followed these conditions. Consistent with the experiments, 50% of the PAs (54/108) in this structure were polymerized by attaching the polymer chain. Each polymer chain consisted of 100 NIPAM monomers, 2 spiropyrans (SP or MCH depending on light conditions) and 2.8 cross-linkers (averaged number over all polymer chains). The covalent cross-linker was modeled as a P3 type bead using the "intermolecular_interactions" option in Gromacs 2018[14,15]. The simulation box was 50 nm × 50 nm × 5.7 nm for the VVEE-hybrid system which allows the fiber's elongation along the z axis, while in the EEEE-hybrid system, a cubic box was applied. To reduce computational cost, the hybrid systems were first pre-equilibrated to allow the polymer chain to curve and then put into the cubic box. In this way the initial 50

× 50 ×50 nm^3 cubic box can be reduced to 38 nm × 38 nm × 38 nm. Stiff (10%CR) and soft (2.8CR) control systems were also simulated in which 54 polymer chains were randomly distributed with initial dimensions of 30 nm × 30 nm × 30 nm (**Figure S7**). The Martini polarizable water model[16] was applied to solvate the system and Na^+ and Cl^- counterions were added to neutralize the charges of the system.

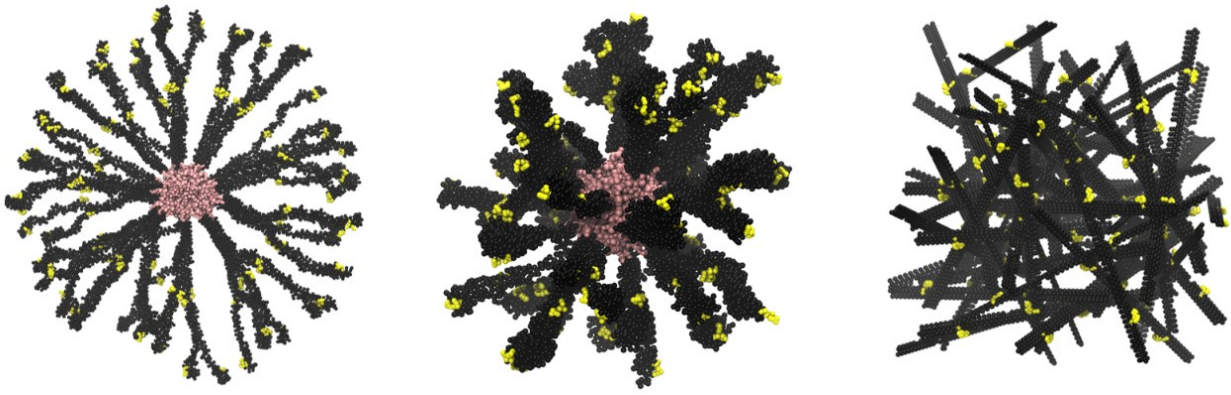

Figure S8. Top view of initial conformations of VVEE-hybrid polymer (left), EEEE-hybrid (middle), control system (right). The PAs are colored in pink, the peptide sequence is colored in black, MCH molecules are colored in yellow. Water and ions are omitted for clarity.

All coarse-grained simulations were conducted using the GROMACS 2018.1 package[14,15]. We first performed a 5000 steps initial relaxation by carrying out a steepest-descent minimization method, followed by a 5 ns NVT ensemble simulation at a temperature of 298 K using a Berendsen thermostat. PA monomers were constrained in the positions obtained from the minimization step while polymer chain relaxed. We then removed the constraints and conducted another 30 ns NPT ensemble simulation at 310 K to further relax the system. The simulation time step was set to be 20 fs and the pressure was set to be 1 bar. At the end of each equilibrium step, a harmonic potential with equilibrium bond length of 0.33 nm and force constant of 5000 kJ/mol/nm^2 were applied to any cross-linkers with a distance less than 1 nm[12]. Once made, the bond was assumed not to break anymore. Next, we performed a production run for 1.5-2.5 μs at 298 K and 1.0 atm. The velocity-rescaling thermostat and Parrinello−Rahman method were used to maintain the simulation temperature and pressure, respectively. The cutoff for the Lennard–Jones potential was 12 Å and the Lennard–Jones potential was smoothly shifted to zero between 9 Å and 12 Å. The cutoff used for the Coulombic potential was also 12 Å. For electrostatic interactions, we used the group method with dielectric constant of 2.5, which is appropriate for the polarizable Martini water model. A Verlet cutoff scheme was used for the neighbor search. Martini constraints were handled using the LINCS algorithm[17]. Periodic boundary conditions were applied in all directions. To guarantee the statistical accuracy and show the reproducibility of our simulations, each hybrid simulation was repeated three times by changing the initial randomized velocities, while each control system was repeated twice.

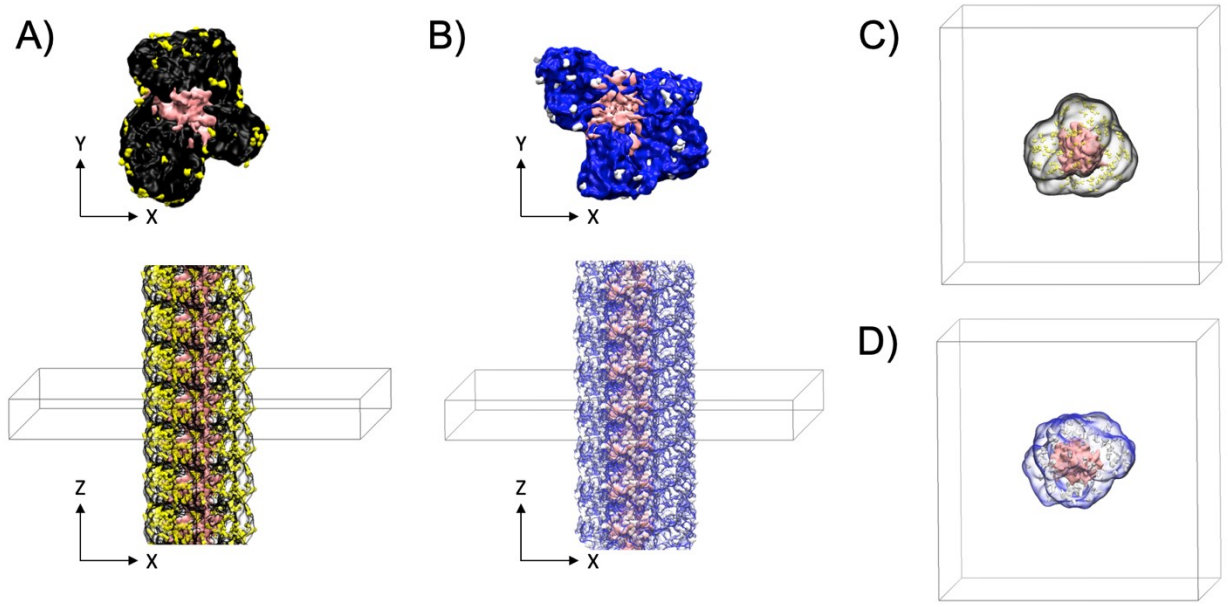

Figure S9. Snapshots of final simulated structures of VVEE (A-B) and EEEE (C-D) hybrid systems, respectively. Top (top panel) and side (bottom panel) views of our high-aspect-ratio supramolecular polymer are shown in A and B, where the hybrids are infinitely long in the Z axis. MCH form-PNIPAM is shown in black, SP form-PNIPAM in blue; PA assemblies in pink; MCH molecules in yellow; SP moieties in gray, and the simulation box is shown in a gray frame, periodic boundary image along the Z axis is shown in Figure A and B. Polymers in Figure C-D, as well as polymers in the bottom panel of Figures A and B, are shown as semi-transparent so that PA structures inside can be seen.

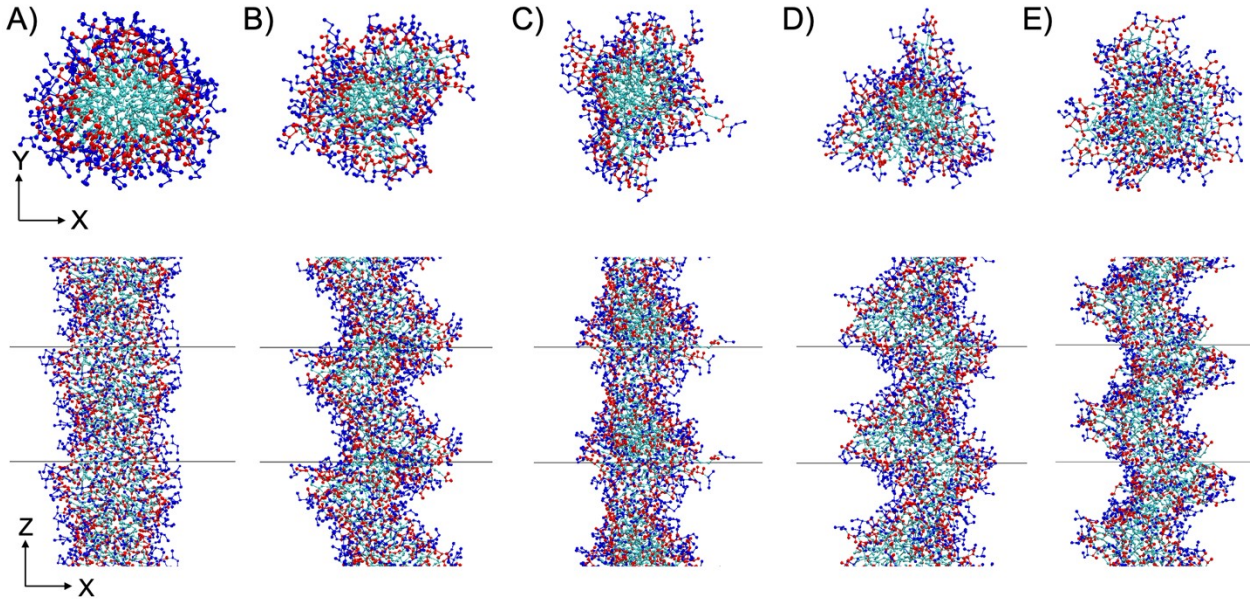

Figure S10. Snapshots of the initial (A) and final morphologies (B-E) of PA in the VVEE hybrid systems, where B, C, D, and E correspond to the VVEE hybrid system containing MCH^{+}, SP, MCH^{-}, and SP^{2-} moieties, respectively. The hydrophobic core of PA is shown in cyan, while the valine is shown in red, and the glutamic acid is shown in

blue. Top view and side view of the PA structures are shown in the top and bottom panels, respectively. Gray horizontal lines show the periodic boundaries along Z.

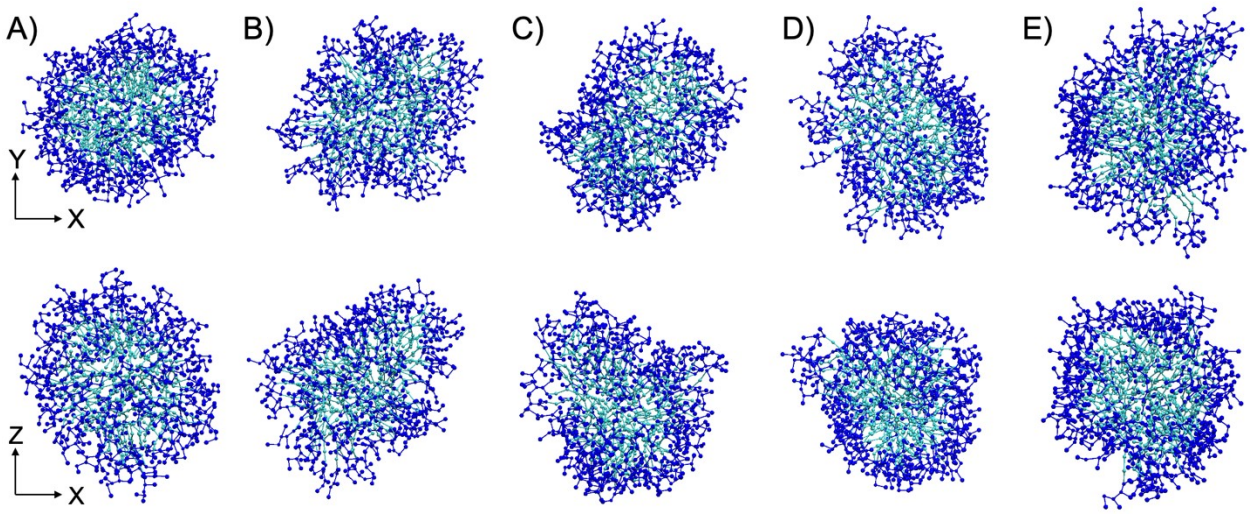

Figure S11. Snapshots of the initial (A) and final morphologies (B-E) of PA in the EEEE hybrid systems, where B, C, D, and E correspond to VVEE hybrid system containing MCH^{+}, SP, MCH^{-}, and SP^{2-} moieties, respectively. The hydrophobic core of the PA is shown in cyan while the glutamic acid is shown in blue. Top view and side view of the PA structures are shown in the top and bottom panels, respectively.

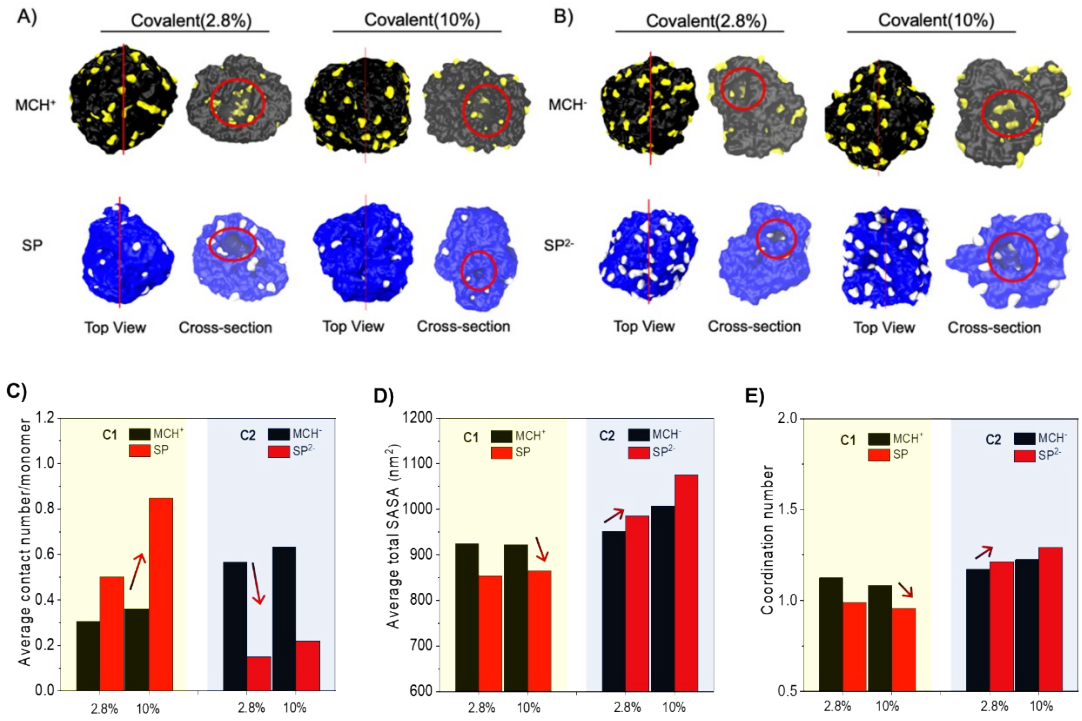

Figure S12. Snapshots of the final simulation structures of covalent control polymers (2.8% and 10%) containing C1(A) and C2 (B). Visible water holes in the cross-section view are marked by red circles. Water and ions are omitted for clarity. **(C)** Average MCH or SP contacts involved within each polymer chain containing C1 (left) and C2 (right). Two MCH (or SP) neighbors form a contact if their interatomic separation is shorter than 0.7 nm. Arrows indicate changes in the y value between merocyanine and spiropyran form upon irradiation. **(D)** Averaged value of the solvent accessible surface area (SASA) for total polymer systems containing C1 (left) and C2 (right). **(E)** Coordination number of water beads found in the first solvation shell of RDF. Data in (E-G) were averaged over the last 200 ns of each simulation.

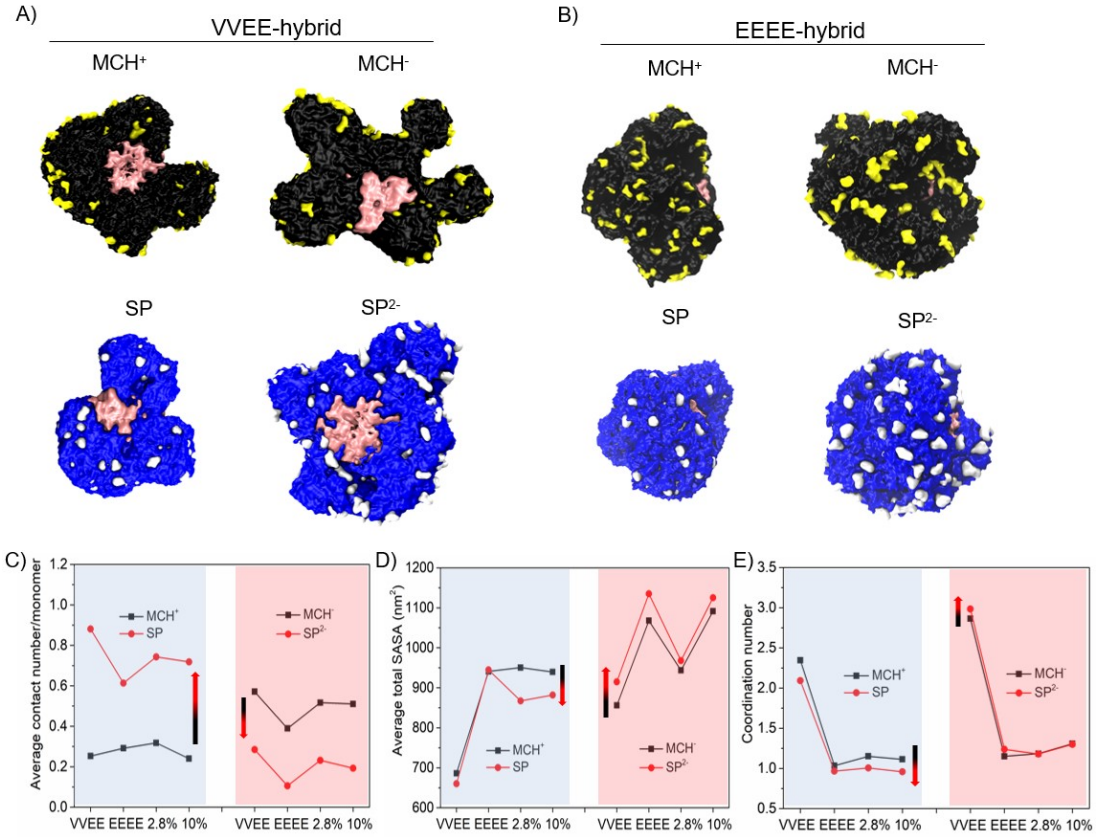

Figure S13. Results of the second set of simulations for the hybrid polymer. Snapshots of the final simulation structures of VVEE (A) and EEEE (B) hybrid polymers containing C1(left) and C2 (right). The MCH form-PNIPAM are shown in blue while SP form-PNIPAM are shown in black. PA assemblies are shown in pink, molecules in the MCH form are in yellow and SP moieties are shown in white (water and ions are omitted for clarity). **(C)** Average MCH or SP contacts involved within each polymer chain. Two MCH (or SP) neighbors form a contact if their interatomic separation is shorter than 0.7 nm. Arrows indicate changes in the contact number between the merocyanine and spiropyran forms upon irradiation. **(D)** Average value of the solvent accessible surface area (SASA) for total polymer systems. **(E)** Coordination number of total polymer and water beads obtained from the ensemble average on atom number within the nearest-neighboring shell.

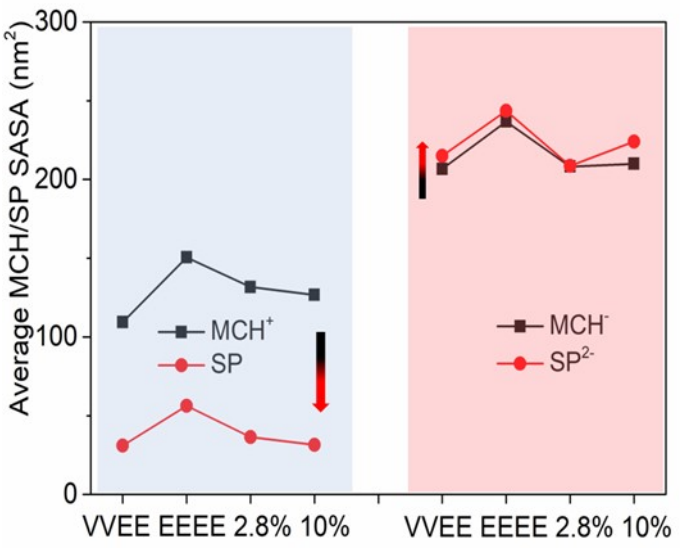

Figure S14. Average value of solvent accessible surface area (SASA) for merocyanine (MCH) and spiropyran (SP) molecules.

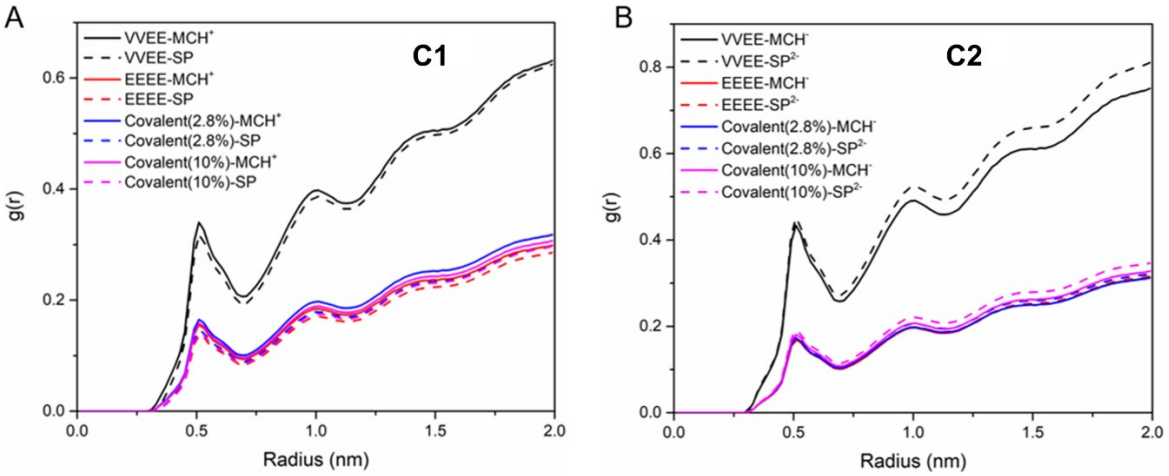

Figure S15. (A-B) Radial distribution function of the polymer and water molecules averaged over the last 200 ns of each simulation. Polymer containing C1 (A) and polymer containing C2 (B). The MCH form is shown with a solid line while the SP form is shown with a dash line. VVEE, EEEE hybrid, covalent (2.8% crosslinker) and covalent (10% crosslinker) polymers are marked in black, red, blue, magenta colors, respectively.

.

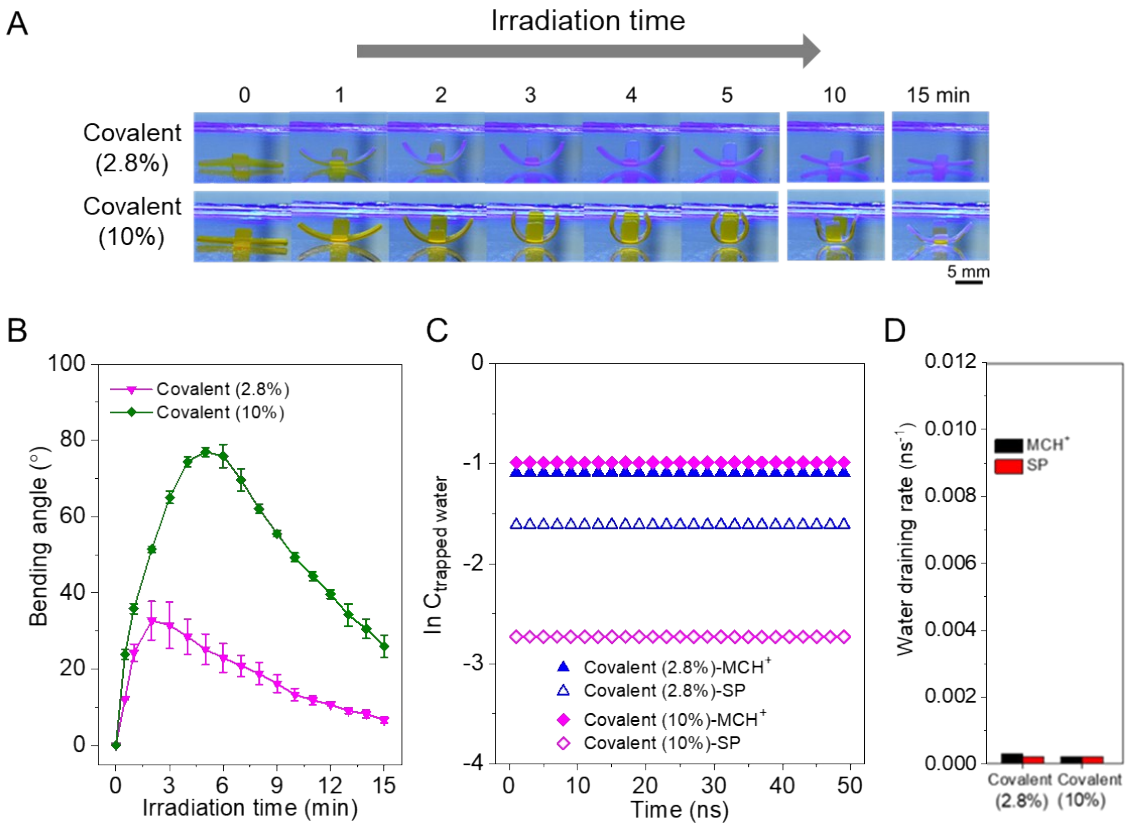

Figure S16. **(A)** Photographs of bending and flattening of different cross-shaped covalent hydrogel films (0.5 mm thick) containing C1 upon irradiation with continuous blue light from top (450 nm, 120 mW/cm^2). **(B)** Plot of bending angles of covalent films containing C1with different crosslinking density. **(C)** Plot of the time evolution of concentration of trapped water (plotted on a logarithmic scale) for pure covalent polymers containing C1 obtained from simulation. **(D)** Plot of the fitted water draining rate for pure covalent polymers containing C1 obtained from linear fitting of data in (C).

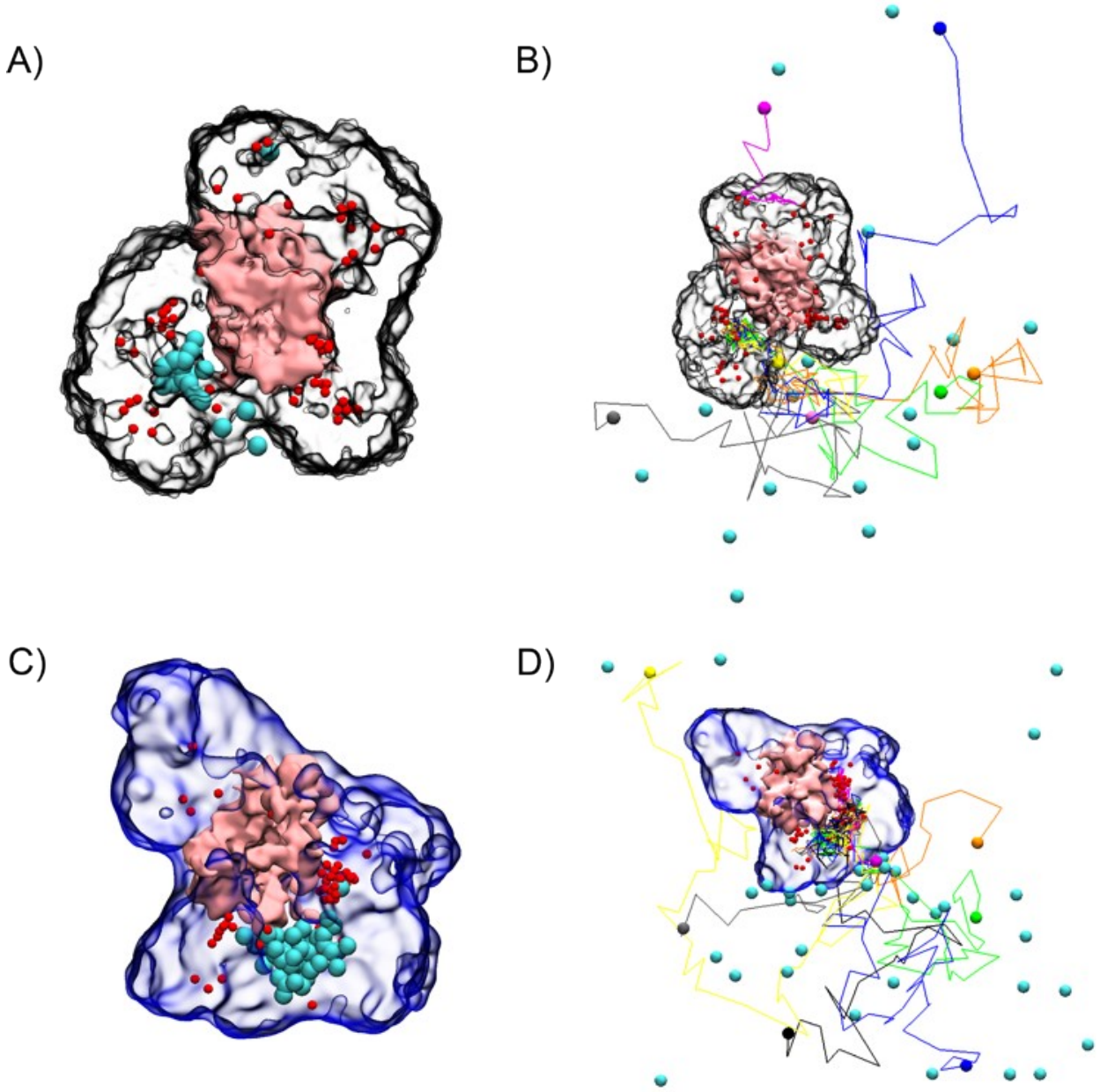

Figure S17. Snapshots of trapped water in VVEE hybrid containing MCH^{+} (A-B) and SP (C-D). All figures were collected from the last 90 ns of the simulation, where figures A and C are from the 40 ns time point, and figures B and D are from the 90 ns time point. The red and cyan beads in figures A and C represent water that is trapped in the hybrid for 40 ns, while the cyan beads represent the water that will escape in the next 50ns. The different colored lines in Figures B and D represent the most representative escaping water pathways selected from all pathways. MCH form-PNIPAM is shown in a black transparent bubble, SP form-PNIPAM in a blue transparent bubble; PA assemblies in pink; MCH and SP moieties are omitted for clarity.

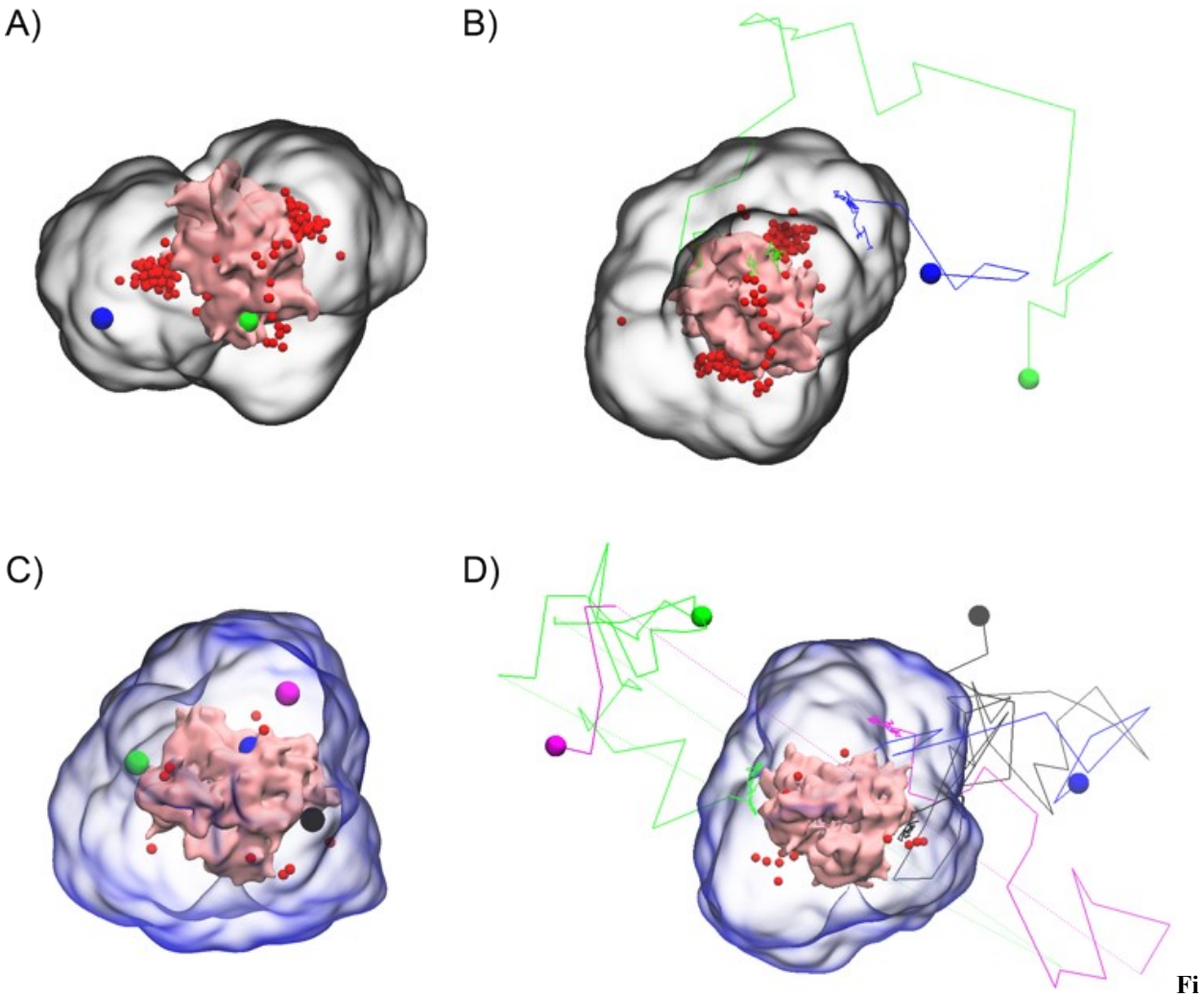

Figure S18. Snapshots of trapped water in EEEE hybrid containing MCH^{+} (A-B) and SP (C-D). All figures were collected from the last 90 ns of the simulation, where figures A and C are from the 40 ns time point, and figures B and D are from the 90 ns time point. The beads in figures A and C represent water that is trapped in the hybrid for 40 ns, while larger represent the water that will escape in the next 50ns. The different colored lines in Figures B and D represent the escaping water pathways. MCH form-PNIPAM is shown in a black transparent bubble, SP form-PNIPAM in a blue transparent bubble; PA assemblies in pink; MCH and SP moieties are omitted for clarity.

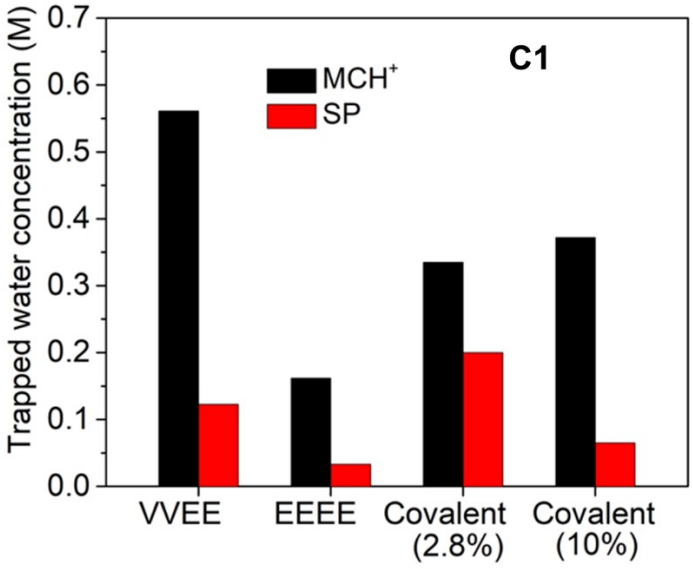

Figure S19. Final concentration of trapped water in C1 systems. Trapped water was defined as water molecules that remain within 10 Å of the polymers for over 40 ns.

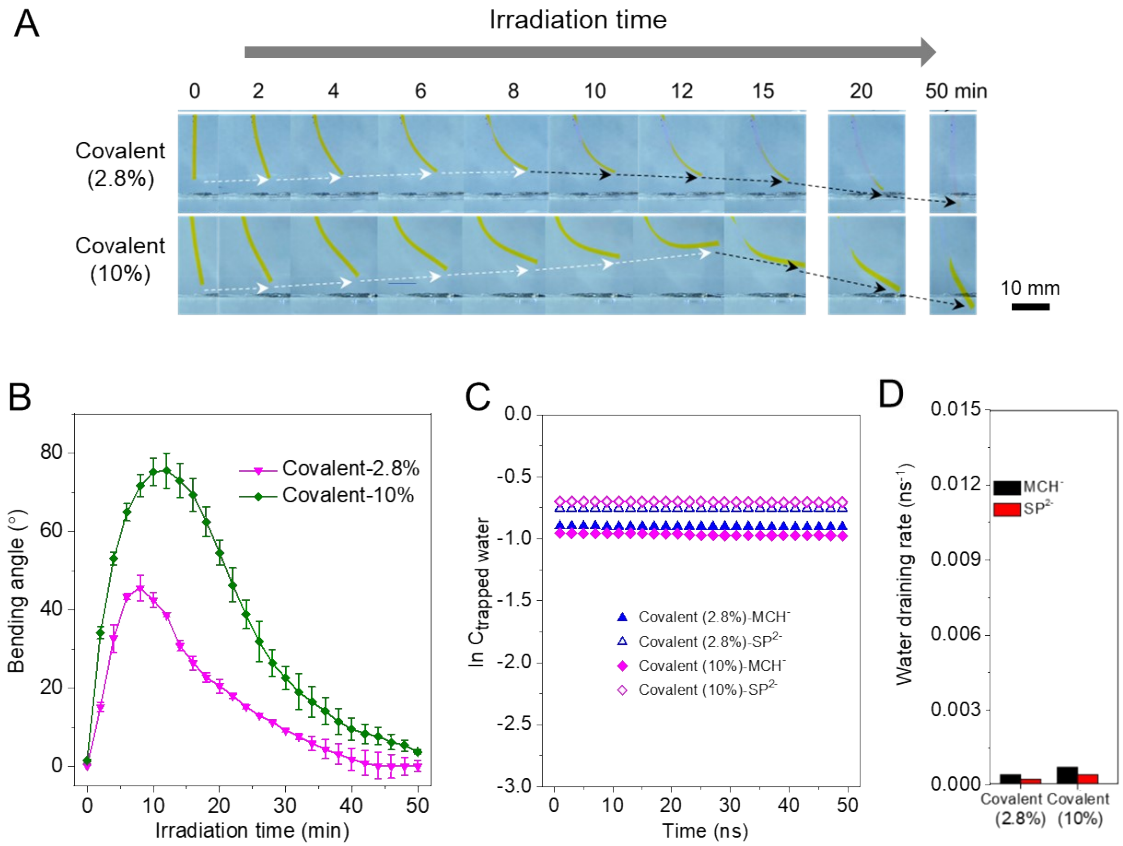

Figure S20. **(A)** Photographs of bending rod hydrogels containing C2 upon irradiation with continuous blue light from left (450 nm, 15 mW/cm^2). **(B)** Plot of bending angles of pure covalent hydrogels containing C2. **(C)** Time evolution of concentration of trapped water for pure covalent polymers containing C2 obtained from simulation. **(D)** Fitted water draining rate for pure covalent polymers containing C2 obtained from linear fitting of data in (C).

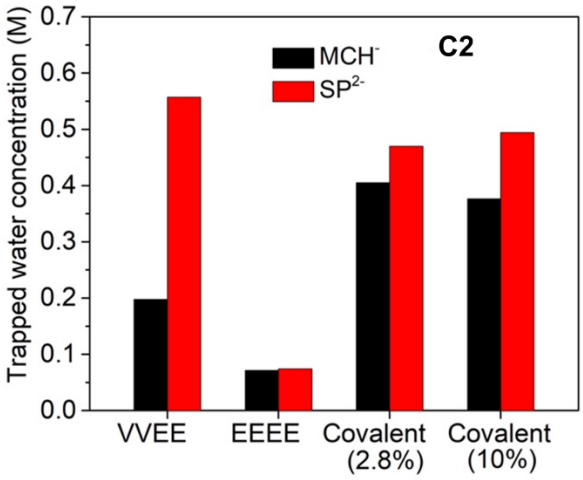

Figure S21. Final concentration of trapped water in C2 systems. Trapped water was defined as water molecules that remain within 10 Å of the polymers for over 40 ns.

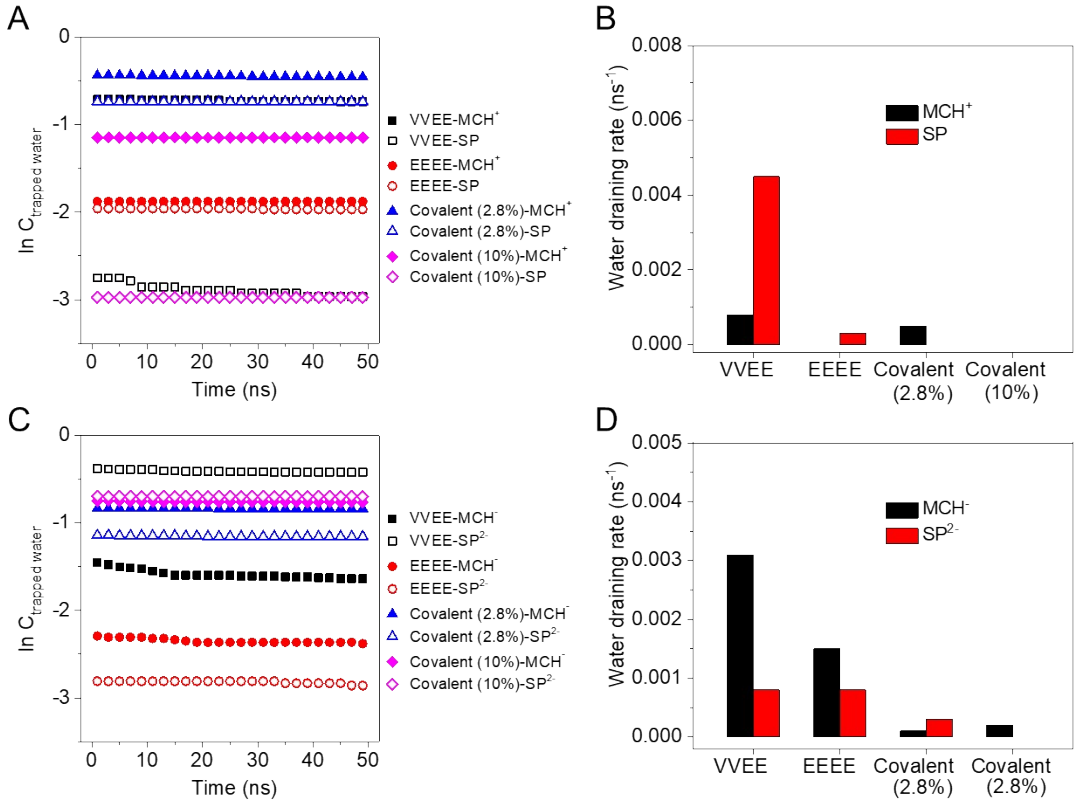

Figure S22. Results of the second set of simulations for hybrid polymer. **(A)** Time evolution of concentration of trapped water for VVEE, EEEE hybrid polymers and covalent polymer containing C1. **(B)** Fitted water draining rate for VVEE, EEEE hybrid polymers and covalent polymer containing C1. Decay rate was fitted based on the plot on a logarithmic scale of first-order decay equation. **(C)** Time evolution of concentration of trapped water for VVEE, EEEE

hybrid polymers and covalent polymer (2.8% and 10%) containing C2. **(D)** Fitted water draining rate for VVEE, EEEE hybrid polymers and covalent polymer (2.8% and 10%) containing C2.

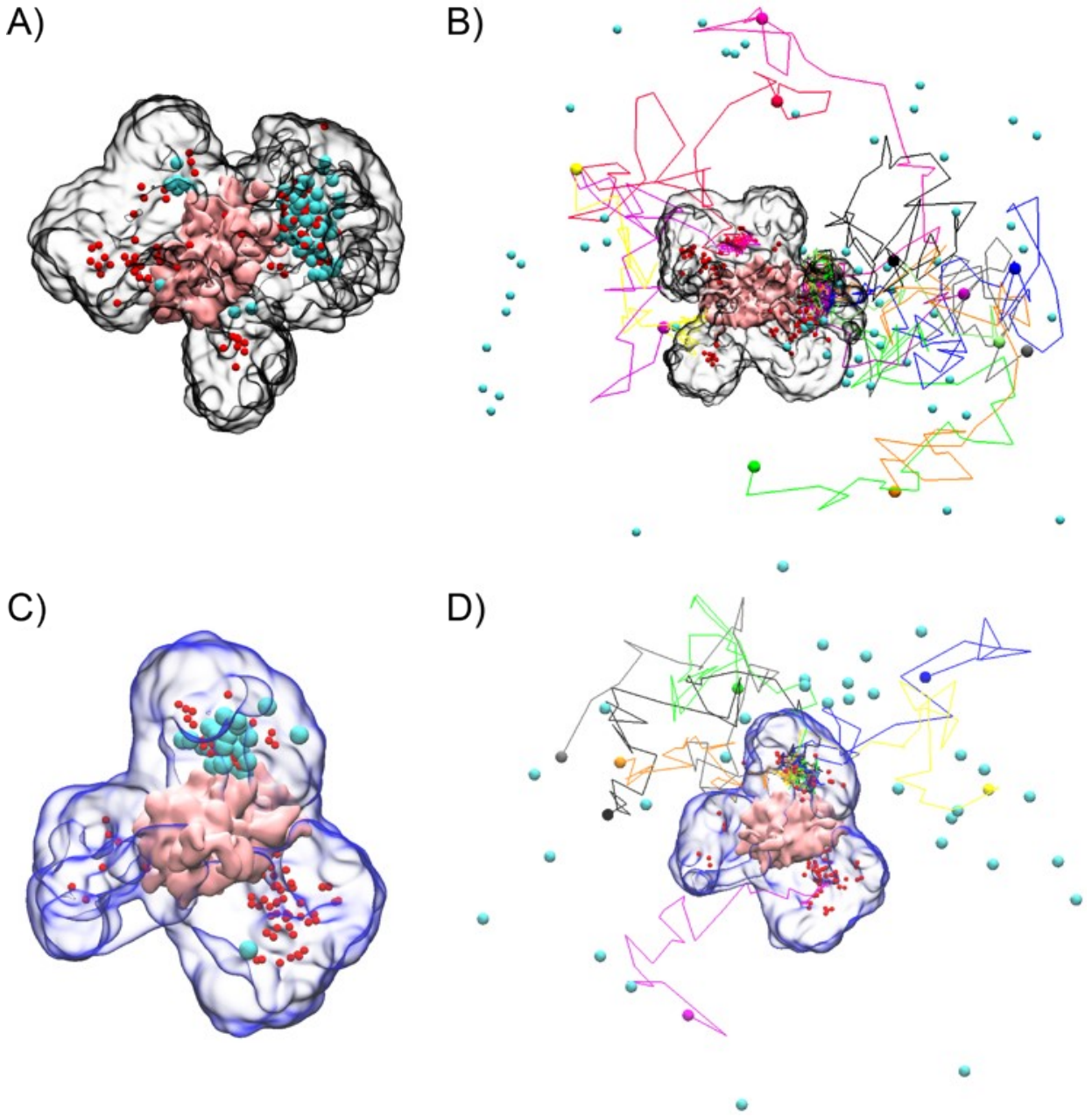

Figure S23. Snapshots of trapped water in VVEE hybrid containing MCH^{-} (A-B) and SP^{2-} (C-D). All figures were collected from the last 90 ns of the simulation, where figures A and C are from the 40 ns time point, and figures B and D are from the 90 ns time point. The red and cyan beads in figures A and C represent water that is trapped in the hybrid for 40 ns, while the cyan beads represent the water that will escape in the next 50ns. The different colored lines in Figures B and D represent the most representative escaping water pathways selected from all pathways. MCH form-PNIPAM is shown in a black transparent bubble, SP form-PNIPAM in a blue transparent bubble; PA assemblies in pink; MCH and SP moieties are omitted for clarity.

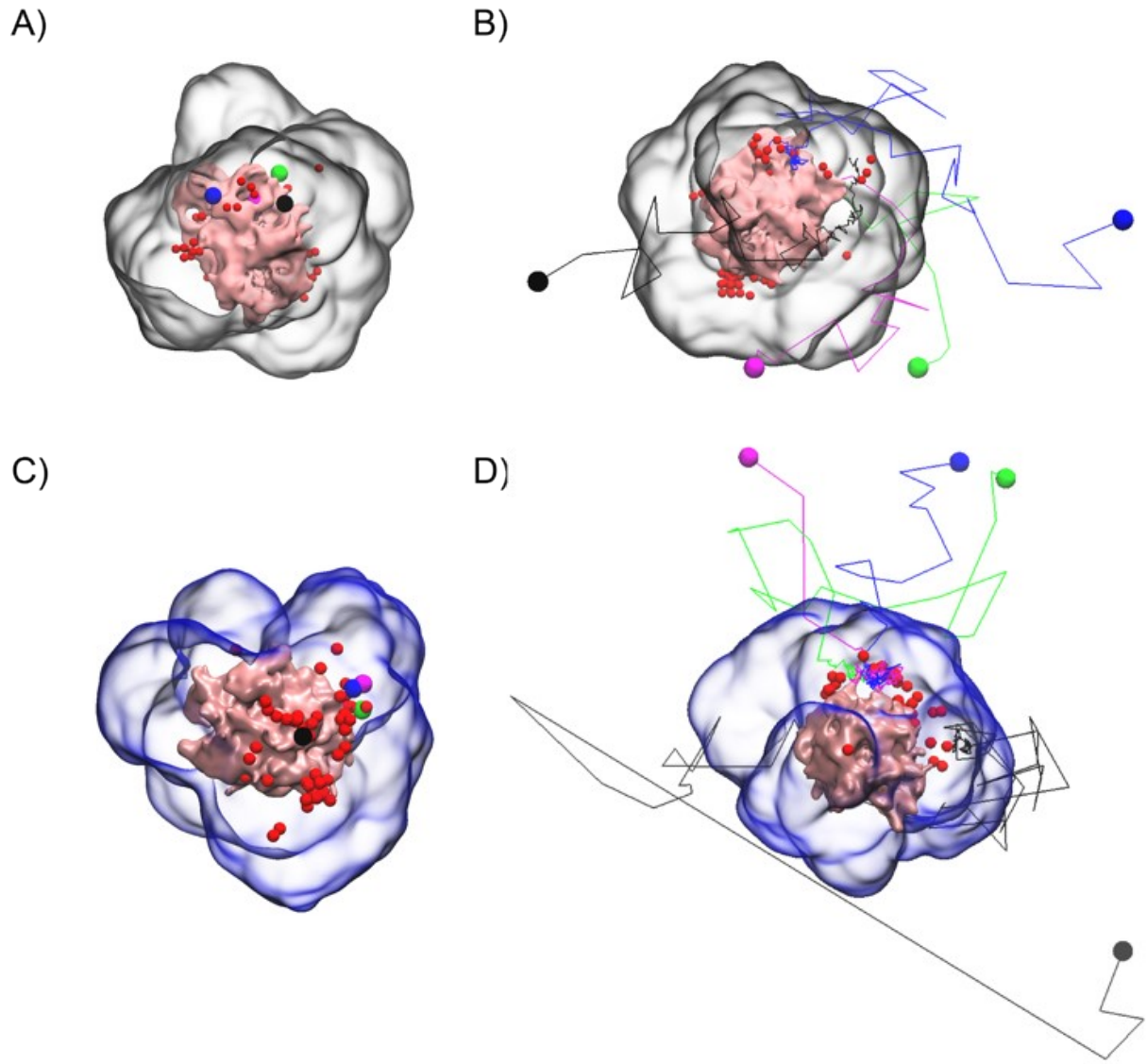

Figure S24. Snapshots of trapped water in EEEE hybrid containing MCH^- (A-B) and SP^{2-} (C-D). All figures were collected from the last 90 ns of the simulation, where figures A and C are from the 40 ns time point, and figures B and D are from the 90 ns time point. The beads in figures A and C represent water that is trapped in the hybrid for 40 ns, while larger represent the water that will escape in the next 50ns. The different colored lines in Figures B and D represent the escaping water pathways. MCH form-PNIPAM is shown in a black transparent bubble, SP form-PNIPAM in a blue transparent bubble; PA assemblies in pink; MCH and SP moieties are omitted for clarity.

Section 5. Characterization of photoactuation behavior

5.1 Photoactuation of C1 hydrogels

The C1 hydrogel thin films (0.5 mm thick) were equilibrated in 5 mM of HCl aqueous solution followed by cutting into a cross shape (each arm is 7 mm long and 3 mm wide) using a blade. The cross-shaped samples were transferred to a large water tank containing 5 mM HCl and irradiated with blue light (450 nm, 120 mM/cm^2) from the top with a distance of 10.5 cm. This light intensity was optimized to guarantee

each sample displays stable bending behavior. For each observation, snapshots were taken from the front view every 5 s using a Nikon digital camera and the bending angles were calculated by ImageJ software.

5.2 Photoactuation of C2 hydrogels

We first tried to study the photoactuation behavior of the C2 expanding hydrogels using the same cross shape as with the C1 samples. However, we failed to obtain a stable bending process because the expanded C2 hydrogels after light irradiation stuck to the glass substrate of the water tank, therefore causing each arm to bend asynchronously and non-reproducibly. In order to avoid this substrate effect, we instead used a rod shape C2 hydrogel, hanging it from the top to study its bending behavior. The light source was a blue LED (Luxeon Star, 450 nm) gooseneck lamp irradiating from left with a distance of 6.5 cm, and the intensity was optimized to be 15 mW/cm^2. For each sample, snapshots were taken from the front view every 5 s using a Nikon Digital Camera and the bending angles were calculated from the photographs using ImageJ software.

References

(1) Lee, O. S.; Stupp, S. I.; Schatz, G. C. Atomistic Molecular Dynamics Simulations of Peptide Amphiphile Self-Assembly into Cylindrical Nanofibers. *J. Am. Chem. Soc.* **2011**, *133* (10), 3677–3683.

(2) Martinez, L.; Andrade, R.; Birgin, E. G.; Martínez, J. M. PACKMOL: A Package for Building Initial Configurations for Molecular Dynamics Simulations. *J. Comput. Chem.* **2009**, *30* (13), 2157–2164.

(3) Humphrey, W.; Dalke, A.; Schulten, K. VMD: Visual Molecular Dynamics. *J. Mol. Graph.* **1996**, *14* (1), 33–38.

(4) Jorgensen, W. L.; Chandrasekhar, J.; Madura, J. D.; Impey, R. W.; Klein, M. L. Comparison of Simple Potential Functions for Simulating Liquid Water. *J. Chem. Phys.* **1983**, *79* (2), 926–935.

(5) Best, R. B.; Zhu, X.; Shim, J.; Lopes, P. E. M.; Mittal, J.; Feig, M.; MacKerell, A. D. Optimization of the Additive CHARMM All-Atom Protein Force Field Targeting Improved Sampling of the Backbone φ, ψ and Side-Chain X1 and X2 Dihedral Angles. *J. Chem. Theory Comput.* **2012**, *8* (9), 3257–3273.

(6) Phillips, J. C.; Braun, R.; Wang, W.; Gumbart, J.; Tajkhorshid, E.; Villa, E.; Chipot, C.; Skeel, R. D.; Kalé, L.; Schulten, K. Scalable Molecular Dynamics with NAMD. *J. Comput. Chem.* John Wiley and Sons Inc. 2005, pp 1781–1802.

(7) Feller, S. E.; Zhang, Y.; Pastor, R. W.; Brooks, B. R. Constant Pressure Molecular Dynamics Simulation: The Langevin Piston Method. *J. Chem. Phys.* **1995**, *103* (11), 4613–4621.

(8) Martyna, G. J.; Tobias, D. J.; Klein, M. L. Constant Pressure Molecular Dynamics Algorithms. *J. Chem. Phys.* **1994**, *101* (5), 4177–4189.

(9) Darden, T.; York, D.; Pedersen, L. Particle Mesh Ewald: An N·log(N) Method for Ewald Sums in Large Systems. *J. Chem. Phys.* **1993**, *98* (12), 10089–10092.

(10) Lee, O. S.; Cho, V.; Schatz, G. C. Modeling the Self-Assembly of Peptide Amphiphiles into Fibers Using Coarse-Grained Molecular Dynamics. *Nano Letters* **2012**, *12* (9), 4907–4913.

(11) Li, C.; Iscen, A.; Sai, H.; Sato, K.; Sather, N. A.; Chin, S. M.; Álvarez, Z.; Palmer, L. C.; Schatz, G. C.; Stupp, S. I. Supramolecular–Covalent Hybrid Polymers for Light-Activated Mechanical Actuation. *Nat. Mater.* **2020**, *19* (8), 900–909.

(12) Li, C.; Iscen, A.; Palmer, L. C.; Schatz, G. C.; Stupp, S. I. Light-Driven Expansion of Spiropyran Hydrogels. *J. Am. Chem. Soc.* **2020**, *142* (18), 8447–8453.

(13) Marrink, S. J.; Risselada, H. J.; Yefimov, S.; Tieleman, D. P.; De Vries, A. H. The MARTINI Force Field: Coarse Grained Model for Biomolecular Simulations. *J. Phys. Chem. B* **2007**, *111* (27), 7812–7824.

(14) Abraham, M. J.; Murtola, T.; Schulz, R.; Páll, S.; Smith, J. C.; Hess, B.; Lindah, E. Gromacs: High Performance Molecular Simulations through Multi-Level Parallelism from Laptops to Supercomputers. *SoftwareX* **2015**, *1–2*, 19–25.

(15) Lemkul, J. From Proteins to Perturbed Hamiltonians: A Suite of Tutorials for the GROMACS-2018 Molecular Simulation Package [Article v1.0]. *Living J. Comp. Mol. Sci.* **2019**, *1* (1), 1–53.

(16) Yesylevskyy, S. O.; Schäfer, L. V.; Sengupta, D.; Marrink, S. J. Polarizable Water Model for the Coarse-Grained MARTINI Force Field. *PLoS Comput. Biol.* **2010**, *6* (6), e1000810.

(17) Hess, B.; Bekker, H.; Berendsen, H. J. C.; Fraaije, J. G. E. M. LINCS: A Linear Constraint Solver for Molecular Simulations. *J. Comput. Chem.* **1997**, *18* (12), 1463–1472.